Project Title:	MIRACLE - Microscopic Image Processing Analysis Coding and Modelling Environment
Contract No:	PIRSES-GA-2009-247091
Instrument:	FP7 PEOPLE Marie Curie Actions IRSES
Thematic Priority:	Medical image processing
Start of project:	1 May 2010
Duration:	36 months

Deliverable No: D6

Segmentation methods for Follicular Lymphoma images

Due date of deliverable:	30 November 2011
Actual submission date:	31 January 2012
Version:	1
Main Authors:	N. Grammalidis, K.Dimitropoulos M. Gurcan, N. Rajpoot, A. Suhre, A. E. Cetin.

Project ref. number	PIRSES-247091
Project title	MIRACLE - Microscopic Image Processing Analysis Coding and Modelling Environment

Deliverable title	Report on segmentation methods for Follicular Lymphoma (FL) images.
Deliverable number	D6
Deliverable version	V1
Previous version(s)	-
Contractual date of delivery	30 November 2011
Actual date of delivery	31 January 2012
Deliverable filename	
Nature of deliverable	Report
Dissemination level	Public
Number of pages	30
Workpackage	2
Partner responsible	ITI-CERTH
Author(s)	N. Grammalidis, K. Dimitropoulos, M. Gurcan, N. Rajpoot, A. Suhre, A. E. Cetin.
Editor	Alexander Suhre
EC Project Officer	Alexandra Pedersen

Abstract	A literature review and case study for follicular lymphoma image segmentation.
Keywords	Microscopic images, Segmentation

Introduction

Follicular lymphoma (FL) is one of the most common lymphoid malignancies in the western world. FL has a variable clinical course, and important clinical treatment decisions for FL patients are based on histological grading, which is done by manually counting the large malignant cells called centroblasts (CB) in ten standard microscopic high-power fields from H&E-stained tissue sections. This method is tedious and subjective; as a result, suffers from considerable inter- and intra-reader variability even when used by expert pathologists. Automatic, computer vision driven techniques will greatly increase the accuracy of FL diagnosis of a given sample, when monitored by an experienced medical practitioner. One of the most frequently applied strategies to design such a system, is to mimic the steps of a pathologist, i.e., extracting large malignant cells called centroblasts and counting them. For this task, segmentation of the image is crucial. This report's aim is two-fold:

a) Looking at the state of the art of FL-image segmentation,
b) Presenting a case study.

1. State of the art

1.2 Segmentation in histopathology images

A large focus of pathological image analysis has been on the automated analysis of cytology imagery. Since cytology imagery often results from the least invasive biopsies (e.g., the cervical Pap smear), they are some of the most commonly encountered imagery for both disease screening and biopsy purposes. Additionally, the characteristics of cytology imagery, namely the presence of isolated cells and cell clusters in the images and the absence of more complicated structures such as glands make it easier to analyze these specimens compared to histopathology. For example, the segmentation of individual cells or nuclei is a relatively easier process in such imagery since most of the cells are inherently separated from each other.

Histopathology slides, on the other hand, provide a more comprehensive view of disease and its effect on tissues, since the preparation process preserves the underlying tissue architecture. As such, some disease characteristics, e.g., lymphocytic infiltration of cancer, may be deduced only from a histopathology image. Additionally, the diagnosis from a histopathology image remains the 'gold standard' in diagnosing considerable number of diseases including almost all types of cancer [3]. The additional structure in these images, while providing a wealth of information, also presents a new set of challenges from an automated image analysis perspective. It is expected that the proper leverage of this spatial information will allow for more specific characterizations of the imagery from a diagnostic perspective. The analysis of histopathology imagery has generally followed directly from techniques used to analyze cytology imagery. In particular, certain characteristics of nuclei are hallmarks of cancerous conditions. Thus, quantitative metrics for cancerous nuclei were developed to appropriately encompass the general observations of the experienced

pathologist, and were tested on cytology imagery. These same metrics can also be applied to histopathological imagery, provided histological structures such as cell nuclei, glands, and lymphocytes have been adequately segmented (a complication due to the complex structure of histopathological imagery). The analysis of the spatial structure of histopathology imagery can be traced back to the works of Wiend *et al*. [4], Bartels [5] and Hamilton [6] but has largely been overlooked perhaps due to the lack of computational resources and the relatively high cost of digital imaging equipment for pathology. However, spatial analysis of histopathology imagery has recently become the backbone of most automated histopathology image analysis techniques. Despite the progress made in this area thus far, this is still a large area of open research due to the variety of imaging methods and disease-specific characteristics.

1.2 Automated detection and segmentation of histopathology images

One of the pre-requisites to grading or diagnosis of disease in histopathology images is often the identification of certain histological structures such as lymphocytes, cancer nuclei, and glands. The presence, extent, size, shape and other morphological appearance of these structures are important indicators for presence or severity of disease. For instance, the size of the glands in prostate cancer tend to reduce with higher Gleason patterns [7]. Similarly the presence of a large number of lymphocytes in breast cancer histopathology is strongly suggestive of poor disease outcome and survival [8]. Consequently, a pre-requisite to identification and classification of disease is the ability to automatically identify these structures. These approaches can either be global, in which they attempt to simultaneously segment all the structures in the image scene or local approaches which target specific structures.

Another motivation for detecting and segmenting histological structures has to do with the need for counting of objects, generally cells or cell nuclei. Cell counts can have diagnostic significance for some cancerous conditions. Bibbo *et al*. [9] reported 1.1%-4.7% error in cell counts compared to manual counts for Feulgen-stained prostate specimens. Belien *et al*. [10] found 19-42% error in counting mitoses in Feulgen-stained breast tissue sections. In immunohistochemically stained bone marrow biopsies, Markiewicz *et al*. [11] reported 2.8-10.0% difference in counts between manual and automatic methods, while Kim *et al.* [12] found a correlation of 0.98 between manual and automatic counts of immunostained slides of meningiomas. Sont *et al.* [13] found a correlation of 0.98 between automated and semi-automated methods for inflammatory cell counts in immunostained bronchial tissue.

1.2.1. Local, structural Segmentation:

1.2.1.1 Nuclear Segmentation: Numerous works have been conducted [14-16] on segmentation of various structures in breast histopathology images using methodologies such as thresholding, fuzzy c-means clustering and adaptive thresholding [16]. Thresholding tends to work only on uniform images and does not produce consistent results if there is considerable variability within image sets. Watershed algorithms tend to pose the same problem [15] due to variability in image

sets. Active contours are widely used in image segmentation; however, contours enclosing multiple overlapping objects pose a major limitation. In addition, inclusion of other irrelevant objects from the background further complicates the possibility of obtaining a viable segmentation.

The pixel-level analysis of unstained prostate slides by Fourier transform infrared spectroscopy resulted in 94%-100% accuracy in the pixel-level classification of 10 histologic classes as reported by Fernandez *et al*. in [17]. The pixel-level classification of nuclear material by Boucheron *et al*. [18] resulted in performances (equal tradeoff between detection and false alarm rates) of 88-90% for H&E stained breast tissue. The use of automated methods for pixel-level analysis is perhaps more common for immunostained or fluorescently stained specimens. Singh *et al*. [19] reported 98% accuracy in the detection of positive and negative prostate nuclei immunostained for androgen receptor protein expression. Analysis of cytokeratin-stained lymph node sections yielded 95% detection of stained cells as reported by Weaver *et al*. in [20]. However, these studies focus only on finding individual nuclei.

In H&E stained imagery of astrocytomas and bladder tissue, Glotsos *et al.* [21] reported that 94% of nuclei were correctly delineated. Latson *et al*. found 25% poorly segmented nuclei, 4.5%-16.7% clumped nuclei, and 0.4%-1.5% missed nuclei in H&E stained breast biopsies. Fluorescently stained imagery of cervical and prostate carcinomas allowed for 91%-96% accuracy in cell segmentation by Wahlby *et al.* [22], where the accuracy here is calculated based on manual cell counts (i.e., not taking into account the accuracy of the actual nuclear delineation). Korde *et al.* used image intensity thresholding to segment nuclei in the bladder and in skin tissue [23]. Gurcan *et al*. leveraged gray level morphology followed by hysteresis thresholding to achieve cell nuclei segmentation in digitized H&E stained slides [24, 25]. Other algorithms have been proposed using more complex techniques, such an active contour scheme for pap-stained cervical cell images by Bamford and Lovell [26] and a fuzzy logic engine proposed by Begelman, *et al.* [27] for prostate tissue that uses both color and shape based constraints.

In [14, 28] nuclear segmentation from breast and prostate cancer histopathology was achieved by integrating a Bayesian classifier driven by image color and image texture and a shape-based template matching algorithm (Figure 1). Figure 1(a) shows a DCIS study with a number of nuclei closely packed together. The likelihood image representing the probability of each pixel corresponding to a nuclear region is shown in Figure 1(b). Note that several nuclei lie adjacent to each other and hence template matching is used to extricate the individual nuclei. Figure 1(c) shows the result of thresholding the Bayesian likelihood scene (95% confidence level). Template matching is then done at every location in 1(c). Only those image locations where correspondence between the binary segmentation (Figure 1(c)) and the template was found are shown as bright. The final nuclear boundary detection (green dots) is displayed in Figure 1(d).

1.2.1.2. Gland segmentation: In a recently presented scheme for extracting glandular boundaries from histopathology scenes [14], the algorithm consists of three distinct components: In the first stage a Bayesian classifier is trained based on color and textural information to automatically identify nuclei, cytoplasm, and lumen regions in the scene. This information is used to train a supervised classifier to identify candidate nuclear, cytoplasmic, and lumen regions within the histological scene.

Following low-level Bayesian classification, structural constraints are incorporated to constrain the segmentation by using image Information regarding the specific order of arrangement of glandular structures (central lumen, surrounding cytoplasm and nuclear periphery) in order to reduce number of false positive gland regions. Finally, a shape-based segmentation method in the form of level sets [29] is initialized within candidate lumen regions as determined from the Bayesian classifier. Hence the level set surface evolution is controlled by the Bayesian probability scene derived via use of the low-level image information. The level set evolution is stopped at the interface between lumen and cytoplasm and thus a segmentation of the inner gland boundary is obtained. A second level set is then initialized within the cytoplasm area and used to capture the outer gland margin. Once the possible gland lumens are found, boundary segmentation is performed using level-sets. A boundary B evolving in time t and in the 2D space defined by the grid of pixels C is represented by the zero level set B = {(x, y)|f(t, x, y) = 0} of a level set function f, where x and y are 2D Cartesian coordinates of c Î C. The evolution of f is then described by a level-set formulation adopted from [29]:

$$\frac{\partial \phi}{\partial t} + F \mid \nabla \phi \mid = 0 \tag{1.1}$$

where the function *F* defines the speed of the evolution. The curve evolution is driven by the nuclei likelihood image. The initial contour $\phi_0 = \phi$ (0*, x, y*) is initialized automatically using the detected lumen area from the candidate gland regions. The curve is evolved outward from the detected lumen regions in the combined nuclei likelihood image to avoid noise and allow smoother evolution relative to the original image. The intensities of the nuclei likelihood image form the stopping gradient. The algorithm is run until the difference in the contours in two consecutive iterations is below an empirically determined threshold. During training, size distributions similar to those used to calculate object likelihood are created using the final contours. These nuclear boundary based distributions are used to remove regions that are too large to be true glands. Finally, the lumen and nuclear boundaries extracted from true gland regions are passed on to the next step for feature extraction.

1.2.2 Global Scene Segmentation Approaches:

In [31], a unified segmentation algorithm for subcellular compartmentalization was presented. Quantitation of biomarkers at sub-cellular resolution requires segmentation of sub-cellular compartments such as nuclei, membranes, and cytoplasm. While different segmentation algorithms can be used for each of the sub-cellular compartments, an alternative is to use the same algorithm in different modes. The algorithm in [31] captured a set of bright pixels sharing a common shape distribution. The algorithm used a set of three features, one is the fluorescent emission intensity, and the other two are based on curvature descriptors that are computed from the eigenvalues of the Hessian matrix.

For an image, $I(x,y)$, the eigenvalues ($\lambda_1(x,y) \le \lambda_2(x,y)$) of the Hessian matrix encode the curvature information of the image, and provide useful cues for detecting ridge-like membrane structures, or blob-like nuclei structures. However, the eigenvalues are dependent on image brightness. The following two curvature-based features are independent of image brightness:

$$\theta(x,y) = \text{atan2}\left(\lambda_1(x,y), \lambda_2(x,y)\right), \quad (1.2)$$

$$\phi(x,y) = \tan^{-1} \frac{(\lambda_1(x,y)^2 + \lambda_2(x,y)^2)^{1/2}}{I(x,y)}, \quad (1.3)$$

and referred to as shape index, and normalized-curvature index, respectively. This is essentially the same as defining the eigenvalues in a polar coordinate system. This transformation also results in bounded features, $-3\pi/4 \le \theta(x,y) \le \pi/4$, and $0 \le \phi(x,y) \le \pi/2$.

The estimation process starts with the expected distributions of the shape index for the structures to be segmented. For example, for bright membrane and vessel like structures the shape index is close to $-\pi/2$, because the smaller eigenvalue is negative and the larger eigenvalue approaches to zero. On the other hand, for the blob-like nuclei structures, the shape index is close to $-3\pi/4$, because both eigenvalues are negative and close in value. For both structures, positive values indicate a pixel being more like a background. These constraints are used to compute the initial foreground and background sets for membrane and nuclei structures. An initial segmentation based on the shape index and the normalized-curvature index separates the image pixels into three subsets: background, foreground, and indeterminate. The indeterminate subset comprises all the pixels that are not included in the background or foreground subsets. From these subsets, the background and foreground intensity distributions, as well as the intensity log-likelihood functions are estimated. The algorithm keeps iterating by using two out of the three features at a time to estimate the distribution of the feature that is left out. In the final step, these log-likelihood functions are combined to determine the overall likelihood function. A probability map that represents the probability of a pixel being a foreground is calculated.

Cytoplasm can be detected either by using a specific cytoplasmic marker, or can be detected using computational methods using the fact that the cytoplasmic areas are between nuclear and membrane areas. For most cancer tissue types, it is very important to differentiate the epithelial tissue from the stromal and connective tissue, so that for IFC studies the expression levels of most markers in the epithelial regions can be quantified. Computational methods that use the high connectivity of membrane meshes can be used to differentiate the epithelial regions. For the sample images, any connected component larger than 800 pixels is accepted as a part of the epithelial mask. The nuclei set is then separated into epithelial nuclei and stromal nuclei using the epithelial mask.

EMLDA is an image segmentation method, which uses the Fisher-Rao criterion as the kernel of the expectation maximization (EM) algorithm [30]. Typically, the EM-algorithm is used to estimate the parameters of some parameterized distributions, such as the popular Gaussian mixture models, and assign labels to data in an iterative way. Instead, the EMLDA algorithm uses the Linear Discriminant Analysis (LDA), a supervised classification technique, as the kernel of EM-algorithm and iteratively group data points projected to a reduced dimensional feature space in such a way that the separability across all classes is maximized. In [13], authors successfully applied this approach in the context of histopathological image analysis to achieve the segmentation of digitized H&E stained whole-slide tissue sample.

1.2 Segmentation of FL images

In [32], segmentation of follicles is achieved by thresholding the red channel from the RGB input image, using the mean brightness of the channel as the threshold. The density of “foreground” pixels of the resultant binary image is then measured by applying a transform to the image data, which’s output measures the foreground density in four directions.

In [33], a bi-modal Gaussian mixture model is assumed for the distribution of cellular and extracellular regions. The expectation maximization (EM) algorithm is then used for segmentation of the image. Bayes’ rule is then applied to each pixel to find the posterior probability of belonging to either of the two classes. A cellular-likelihood image is found by using a sigmoid function, followed by a locally adaptive thresholding step, which’s end result is a binary representation of the image that represents the final segmentation. To account for unwanted merging of individual cells by the segmentation a fast-radial symmetry transform is applied to the segmentation. When this segmentation scheme is used for centroblast detection, the average accuracy is about 80%.

The approach discussed in [34], is semi-automated procedure, where seed points of the region of interest are provided by the user and are used as starting points for the segmentation. After this step, a filter is applied to the image in order to enhance the contours of the follicle regions. The actual segmentation is then solved by using active contours: starting with an initial curve and evolving it to the “correct” steady state, i.e. the object boundaries. [34] states: “The spatial coordinates (x_s, y_s) of the seed points are each used as the center of the circular curve expanded iteratively inside each follicular region. Applying active contours globally will lead to overlapping areas, which are then very difficult to extract and identify. The initial curve is circular, in general an appropriate estimate of the curvature of the follicle. The circle is then diffused iteratively inside the follicular region. The process converges when the fitting between the curve and the object is achieved. This is based on the minimization of energy between the object and the fitted curve.” As final steps, morphological filters and Fourier descriptors are applied to the binary image, in order to account for irregular contours.

In [35], the authors are concentrating on finding feasible features on which to use k-means and k-nearest-neighbor (KNN) classifiers for classification into two classes (nuclear or extra-cellular regions). Those features are basically local Fourier transform (LFT) features, but those are not computed over the original RGB colorspace, but rather a most discriminative color space (MDC), obtained by Fisher-Rao discriminant analysis. The paper also introduces a computationally efficient way of computing the LFT features. K-means is used for getting a compact representation of the features, while KNN is used for final classification into the desired two classes.

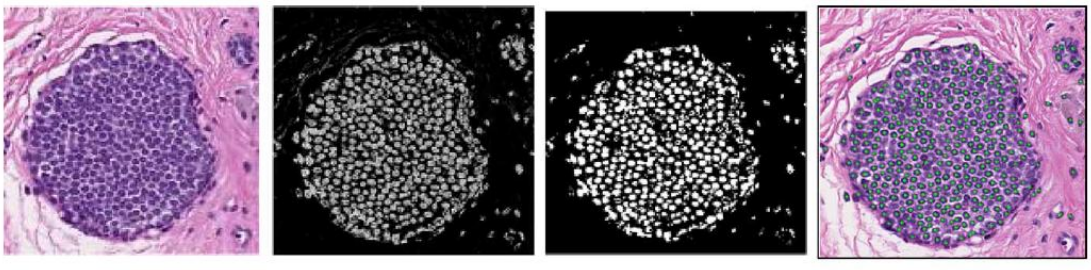

Figure 1: (a) Original DCIS image with corresponding (b) likelihood scene obtained via a Bayesian classifier driven by color and texture. (c) Thresholded version of likelihood scene (95% confidence). (d) The final nuclear segmentation obtained by integrating the Bayesian classifier with the template matching scheme.

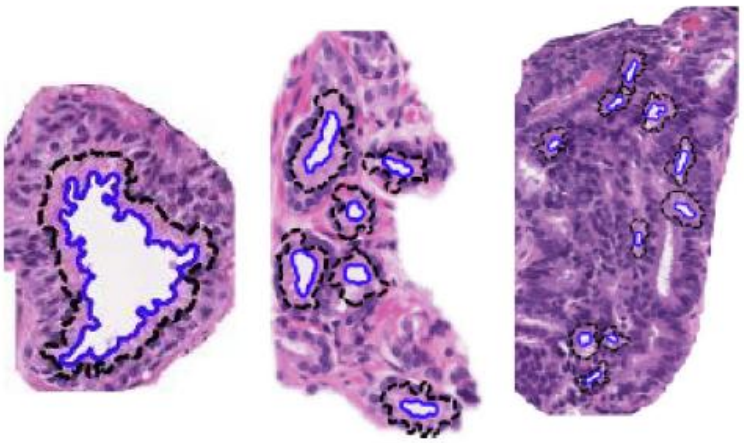

Figure 2: Results of the automatic segmentation algorithm (blue contours: lumen boundary, black contours: inner boundary of the nuclei of the epithelial cells surrounding the gland). Shown from left to right are example images of benign epithelium, intermediate-, and high-grade cancer.

2. A case study: Application and evaluation of different image segmentation techniques for follicular lymphoma image analysis.

2.1 Introduction to medical image segmentation

Segmentation i.e. partitioning of a medical image into multiple segments that are meaningful physical entities/objects is an important step in medical image. Since a large number of medical images with many details need to be processed, manual segmentation is very time consuming, results are not reproducible and may suffer from intra- and inter- observer variability [36]. Compared with standard algorithms used for image processing, the algorithms used for medical images need to satisfy additional constraints, exploit specific a-priori knowledge like properties of the imaging procedure or the properties of the organs structures that are displayed on these images. Furthermore, often the influence of noise that is present in these images need to be taken into account and compensated.

Methods for performing segmentations vary widely depending on the specific application, imaging modality, and other factors [37]. For example, the segmentation of brain tissue has different requirements from the segmentation of the liver. General imaging artifacts can also have significant consequences on the performance of segmentation algorithms. No single segmentation method yields acceptable results for every medical image. Some methods are more general and can be applied to a variety of data, however, methods that are specialized to particular applications can often achieve better performance by taking into account prior knowledge. As a result, the selection of an appropriate approach to a segmentation problem can therefore be a difficult dilemma.

Many different algorithms have been proposed for computer-aided segmentation of medical images. Many authors classify the medical image segmentation algorithms into three broad categories: a)threshold-based techniques, clustering-based

techniques and techniques based on deformable models. A more elaborate taxonomy from [38] is as follows:

1. Thresholding
2. Clustering methods
3. Compression-based methods
4. Histogram-based methods
5. Edge detection
6. Region-growing methods
7. Split-and-merge methods
8. Partial differential equation-based methods
9. Parametric methods
10. Level set methods
11. Graph partitioning methods
12. Watershed transformation
13. Model based segmentation
14. Multi-scale segmentation
15. One-dimensional hierarchical signal segmentation
16. Image segmentation and primal sketch
17. Semi-automatic segmentation
18. Neural networks segmentation

The rest of this report will focus on the segmentation of microscopy images (and more specifically on the follicular lymphoma (FL) images) aiming to extract important features from which automatic detection of malignancy is possible.

2.2 Segmentation of FL microscopy images

The aim of this study is the development of advanced algorithms for segmentation of pathological follicular lymphoma microscopy images as a first step in developing systems to extract important features from which automatic detection and grading of malignancy is possible.

Follicular Lymphoma (FL) is a group of malignancies of lymphocyte origin that arise from lymph nodes, spleen and bone marrow in the lymphatic system in most cases and it is the second most common non-Hodgkin's lymphoma. FL can be differentiated from all other subtypes of lymphoma by the presence of a follicular or nodular pattern of growth presented by follicle center B cells consisting of centrocytes and centroblasts. In practice, FL grading process often depends on the number of centroblasts counted within representative follicles. FL morphology-based histological grading of FL images obtained by microscopy and stained using is very important for the optimal choice of treatment. Tissues are stained using Immunohistochemistry (IHC) or Hematoxylin and Eosin (H&E) *staining* methods. The automation of this procedure has many advantages: the PC yields objective results, so malignancy can be detected easier, and results can be easily stored and used for future studies.

A general image processing chain for IHC and H&E stained microscopic images usually consists of the following steps:

1. A first optional (pre-processing) step image filtering and smoothing operations, such as morphological operators or median filters.
2. Cells are segmented from their background (e.g. collagen).
3. The individual cells are segmented within each cluster.
4. As a post-processing step, segments containing multiple cells are identified and split based on the shape of their segment.

In order to evaluate some state-of-the-art image segmentation approaches, an image processing of microscopic images from H&E-stained tissue sections is proposed (Figure 3), similar to the methodology followed in [46]. Specifically, the following steps are followed:

1. PCA or a simple Colour to Greyscale transform is used to convert the colour image into a Greyscale image.
2. A Gaussian smoothing filter is applied
3. An Image segmentation approach to segment the foreground (cells) from background (collagen).
4. Morphological operations and connected component labelling is used as post-processing
5. A distance transformation followed by a watershed transformation is used to segment merged groups of cells into distinct cells, based on their boundary.

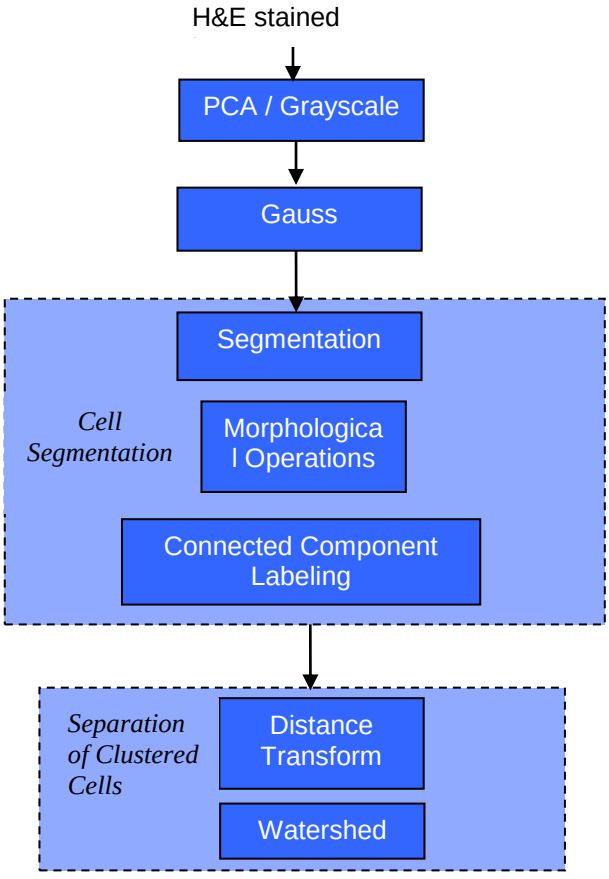

Figure 3: Segmentation of Microscopy Images for follicular lymphoma

In the following, a number of image segmentation techniques are examined in detail, mainly as alternative approaches for Step 3 of the algorithm i.e. the segmentation of the image into two classes, i.e. foreground (cells) and background (collagen). In the following sections, seven state-of-the-art algorithms were applied for this task, namely:

1. Adaptive thresholding (Otsu method)
2. Adaptive thresholding (Kapur's energy maximization method)
3. Iterative thresholding method (Shapiro method)
4. ISODATA algorithm
5. Fuzzy C-means (FCM) clustering
6. Gaussian Mixture Models / EM algorithm
7. Energy Minimization based on Graph Cuts

Finally, results obtained after the procedure to split clustered group of cells (using a distance transform of the resulting binary image followed by a watershed algorithm) are also presented.

2.3 Thresholding Techniques

Thresholding is a useful and simple method for segmenting grey level images and is based on the fact that the foreground objects can be separated from the background based on their grey level values.

The histogram of the image is used and a selection of one or multiple grey level values is made, to be used as threshold(s) between the pixel values of the foreground and the background.

The initial grey level image can be converted to a binary image, so that the image segments which correspond to the foreground (background) are black (white), respectively.

A significant problem for the task of separating pixels in two classes based only on the pixel's grey-level value is how to make an optimal choice for the corresponding threshold. A simple selection may be the mean or median value of the histogram, but this is not always the best choice. To solve this problem, a number of optimal thresholding techniques were evaluated for the segmentation of medical images. In [39], 40 different adaptive thresholding techniques are exhaustively described, categorized and compared for the specific task of image thresholding. We selected two of the best performing techniques in this review as well as an additional technique described in [49], which is reported to be very efficient and has significant advantages. These techniques are presented below.

2.3.1 Adaptive Thresholding method by Otsu

One of the most important and most commonly used adaptive thresholding techniques is the Otsu method. It is based on the processing of the image histogram and the determination of the threshold based on the criterion of maximizing the

separability between the foreground and background regions. For the conversion of a greyscale image into binary, a threshold value t needs to be specified, which can separate the greyscale values into two classes C_0, and C_1 where C_0 {0,1, 2,L, t} and C_1 {t+1,t+2,L, L -1} , where L where L is the total number of grey levels in the image. Each class contains the pixels with values that are lower and higher respectively than the threshold t.
If με n_i are the number of pixels of the i-th grey level and n is the number of pixels in the image, the probability of the i-th grey level is defined as:

$$p_i = \frac{\mathrm{n_i}}{\mathrm{n}}$$

Where C_0 and C_1 correspond to the foreground and background respectively. The probabilities of these two classes are called ω_0 ,ω_1 are calculated as:

$$\omega_{0=} \sum_{i=0}^{t} \mathrm{p_i}$$

$$\omega_{1=} \sum_{i=t+1}^{L-1} \mathrm{p_i}$$

The average grey level values within each class are

$$\mu_0\,(t) = \sum_{i=0}^{t} \mathrm{ip_i}\,/\omega_0(t)\mu_1(t)$$

$$\mu_1\,(t) = \sum_{i=t+1}^{L-1} \mathrm{ip_i}\,/\omega_1(t)$$

An optimal thresholding value can be determined by maximizing the variance between the 2 classes

$$t = \mathrm{Arg}\{\max_{0\le \mathrm{i} \le \mathrm{L}-1} (\frac{\sigma_B^2}{\sigma_T^2})\}$$

where σ_B^2 is the intra-class variance, defined as a weighted sum of variances of the two classes:

$$\sigma_B^2 \ = \omega_0 \ (\mu_0 - \mu_T)^2 + \omega_1(\mu_1 - \mu_T)^2$$

and σ_t^2 is the sum of squares of the standard deviation of the grey level values which is calculated by the formula:

$$\sigma_{\mathrm{T}}^2 = \sum_{i=0}^{L-1} (\mathrm{i} - \mu_T)^{\ 2}$$

where the average grey level value is:

$$\mu_T = \sum_{i=0}^{L-1} \mathrm{ip_i}$$

The steps of the algorithm are as follows:

1. Compute the histogram and the probability of each grey level
2. Initialize values $\omega_i(0)$ and $\mu_i(0)$
3. Step through all possible thresholds t=0,…,L-1

   a. Update values ω_i and μ_i
   b. Compute intra-class variance
4. Choose the threshold that maximizes intra-class variance in b.

2.3.2 Kapur's entropy-based method

This method was proposed by Kapur et al. and is based on the maximization of the entropy of the image. Two probability distributions are used in this method: one for the foreground and one for the background regions. The optimal threshold value T is selected so as to maximize the total entropy of the image, i.e. the sum of the entropy H(B) of the background and H(F) of the foreground.

The probability distribution of the grey levels in the low grey value (dark, foreground) region is:

$$F: \frac{p_o}{P_t}, \frac{p_1}{P_t} \dots \dots . \frac{p_t}{P_T},$$

And in the high grey value (white, background) region:

$$\mathrm{B}: \frac{p_{t+1}}{1-P_t}, \frac{p_{t+2}}{1-P_t} \dots \dots . \frac{p_{L-1}}{1-P_t},$$

where P_t is the probability of pixels with grey level less than or equal of the threshold t

$$\mathrm{P_t} = \sum_{i=0}^{t} \mathrm{p_i}$$

The entropy for the foreground pixels is calculated by the formula:

$$\mathrm{H(F)} = \ln \mathrm{P_t} + \frac{\mathrm{H_t}}{\mathrm{P_t}}$$

Where H_t is calculated by the formula:

$$H_t = -\sum_{i=0}^{t} (\mathrm{p_i} \ln \mathrm{p_i})$$

Similarly, for the background region we can calculate entropy as:

$$\mathrm{H(B)} = \ln(1-\mathrm{P_t}) + \frac{\mathrm{H_{L-1}} - \mathrm{H_t}}{1-\mathrm{P_t}}$$

where H_{L-1} is computed by the formula:

$$H_{L-1} = -\sum_{i=0}^{L-1} (\mathrm{p_i} \ln \mathrm{p_i})$$

And the total entropy of the image is:

$$M\ (t)\ =\ \mathrm{H(O)} + \mathrm{H(B)}$$

The optimal threshold is the value where $M(t)$ is maximized and can be computed by the following steps:

1. We compute the probabilities p_i of the grey levels of the foreground (F) and background (B) classes for each possible threshold t
2. We compute the logarithms of the values of the F and B class
3. We compute the entropy of the F and B classes
4. We compute the total entropy $M\ (t)$ of the image
5. We determine the threshold t that maximizes the total entropy $M\ (t)$

2.3.3 Iterative method by Shapiro

A basic problem in thresholding is the selection of the threshold value. A simple method would use an average value (such as the mean or median value), since if the intensity of a pixel of the foreground is higher than the background, it also should also be higher than this average. However, the above assumption is not always true if the image is noisy. A more sophisticated approach might be to create a histogram of the image pixel intensities and use the valley point as the threshold, however this approach may not be very useful if the histogram does not have a clearly defined valley point. A relatively simple approach, which does not assume any a-priori knowledge about the image, and performs well under the presence of image noise is the following iterative method proposed in [49] by Shapiro:

Algorithm steps

1. A random threshold value is selected.

2. The image is segmented into two sets corresponding to the foreground and background regions:

G1 = {f(m,n):f(m,n)≤T} (foreground pixels)

G2 = {f(m,n):f(m,n)>T} (background pixels)

where f(m,n) is the pixel value of the m-th column and n-th row

3. We compute the average value of each set

m1=average (G1)

m2= average (G2)

4. A new threshold is defined as (m1+m2)/2

5. Go back to step 2 and calculate new values until convergence is achieved

This iterative algorithm is a special one-dimensional case of the k-means clustering algorithm, which has been proven to converge at a local minimum (so the actual results depend on the choice of the initial choice for the threshold).

2.4 Clustering techniques

Clustering techniques partition an image into K clusters. We will focus on the special case where two classes are defined (foreground and background) and we will study four approaches:

1. ISODATA algorithm, which is a variation of the classic k-means clustering algorithm for varying number of classes.
2. Fuzzy C-means (FCM) clustering, where each pixel is not assigned to a class deterministically, but using a fuzzy membership weight.
3. Gaussian mixture models and the EM algorithm, which is similar to K-means clustering
4. Energy minimization approaches based on Graph Cuts

2.4.1 ISODATA algorithm

The ISODATA algorithm [44] is a method of unsupervised classification, which is similar to the k-means algorithm with the main difference that the ISODATA algorithm allows for different number of clusters while the k-means assumes that the number of clusters is fixed a-priori.

Specifically, starting from a random initialization, the ISODATA algorithm splits and merges clusters, according to the parameters set. In every iteration, the following three steps are performed:

1) Cluster centers are randomly placed and pixels are assigned to the class for which the distance to class center is minimal.

2) The standard deviation within each cluster, and the distance between cluster centers is calculated.

3) Clusters are split if their standard deviation is greater than the user-defined threshold. On the other hand, clusters are merged if the distance between them is less than the user-defined threshold.

Multiple iterations are performed until either one of the following criteria is satisfied:

i) the average inter-center distance falls below the user-defined threshold,

ii) the average change in the inter-center distance between iterations is less than a threshold, or

iii) the maximum number of iterations is reached

2.4.2 Fuzzy C-means (FCM) clustering

The Fuzzy C-means (FCM) clustering algorithm in which this segmentation method is based was proposed by J.C. Bezdec [45] and is a non-deterministic data clustering technique. Let $P = \{x_1, x_2, \ldots \ldots x_n\}$ be a dataset of pixels to segment into C classes P_1, P_2, P_c, i.e. $P_1 U\, P_2\, U\, P_c = P$. FCM clustering method aims to minimize an objective function, namely:

$$J(\mathrm{U},\mathrm{V}) = \sum_{i=1}^{c} \sum_{\mathrm{k}=1}^{\mathrm{n}} \mathrm{u}_{\mathrm{ik}}^{\mathrm{m}} \ \|\mathrm{x}_{\mathrm{k}} - v_{\mathrm{i}}\|^{2}$$

where

• x_k are the *n* pixels to be classified

• $V = \{v_1, v_2, \ldots \ldots v_c\}$ are the *c* class centers

• $U = [u_{ik}]$ is an *c* x *n* matrix, where u_{ik} is the membership coefficient of *k-th pixel into class i.* For the membership coefficient of each pixel, we normalize with respect to the sum of the class centers, therefore the elements u_{ik} of matrix *U* satisfy the following relations:

$$0 \leq u_{ik} \leq 1, \quad i = 1, \ldots., c \quad k = 1, \ldots., n$$

$$\sum_{i=1}^{c} u_{ik} = 1, \qquad k = 1 \ldots., n$$

$$0 < \sum_{i=1}^{n} u_{ik} < n, \qquad i = 1 \ldots., c$$

• *m* is an exponential weight coefficient with *m* >1, *m* € R (usually *m* = 2).

Therefore, before the start of the algorithm, the parameters *c* and *m* need to be specified. Then the centers of the *c* classes are initialized either to random points, or to randomly selected points from *P*. After the initialization of matrix $V^{(0)}$ (initial state of matrix *V*) the FCM algorithm consists of the following steps:

1. **Computation of the membership matrix $U^{(a)}$** by the formula:

$$u_{ik} = \frac{[\frac{1}{\|x_k - v_\iota\|^2}]^{1/(m-1)}}{\sum_{j=1}^{c} [\frac{1}{\|x_k - v_\iota\|^2}]^{1/(m-1)}}$$

where ı=1,……c and k=1,… n.

As seen in the above formula, the membership weight of a pixel in a class is inversely proportional to the power (m−1) of the distance of the pixel from the class center.

2. **Computation of the centers $\mathbf{V_i^{(a)}}$ of the classes,** with the formula

$$v_i = \frac{\sum_{k=1}^{n} u_{ik}^m x_{ik}}{\sum_{k=1}^{n} u_{ik}^m}$$

for i=1,……c

3. **Computation of the objective function J $^{(a)}$**
4. **Testing of the termination condition.** Specifically, if the difference between the objective function with respect to its value at the end of the previous iteration is smaller than a threshold value

$$\left|J^{(a)} - J^{(a-1)}\right| \leq \varepsilon$$

or if the number of iterations α is equal to the maximum allowed number of iterations a_{max}, the algorithm is terminated. Otherwise, a new iteration occurs from Step 1, where a =a +1.

The previous iterative procedure will lead to a local minimum of the objective function. However, the discovery of the global minimum generally requires an exhaustive search within the entire space of initial points $V^{(0)}$. However, exhaustive search can be computationally inefficient for data with large variance within high dimensional spaces and large numbers of classes. In the case of FCM, the repetition of the procedure with different starting points each time, most of the times leads to the discovery of the global minimum of the objective function.

Finally, if an application does not need information regarding to the level of participation of each data point (pixel) to all classes, but only about the class that it belongs to, then the point is simply assigned to the class that has the largest membership.

2.4.3 Gaussian mixture models and the EM algorithm

In this algorithm, which was also recently used in [46], the grey level intensity distribution of two target classes (e.g. cellular and extracellular components) is modelled using a Gaussian mixture model. The unknown mixture parameters are the mean and variance of the grey level intensities in each class as well as a mixture weight for each class. The mixture parameters can be estimated using the expectation-maximization (EM) algorithm [40]. The method starts with a random initialization and each iteration consists of two steps: In the expectation (E) step the likelihood with respect to the current estimates is computed and in the maximization (M) step the expected log-likelihood is maximized.

2.4.4 Energy minimization approaches based on Graph Cuts

Many problems in computer vision involve assigning a label (such as disparity in stereo, or a FG/BG label in image segmentation). A common constraint is that the label should vary smoothly everywhere, while preserving sharp discontinuities that may exist, e.g. at object boundaries [50]. A common and robust way of dealing with such problems is energy minimization.

More specifically, the image segmentation problems can be formulated as a labelling problem, which can be effectively be described as an energy minimization problem. Energy typically consists of two terms: a *data consistency term*, that measures the consistency of pixel-to-label correspondence and a *smoothness term* which penalizes situations where neighbouring pixels have different labels. Specifically, the goal is to find a labelling l, which minimizes the following energy equation:

$E(l) = E_{data}(l) + E_{smooth}(l)$

where E_{data} measures the consistency of l with the observed data and E_{smooth} determines the extent to which f is piecewise smooth.

Graph cut techniques have been found to be very efficient for finding good approximations of the global minimum in such energy minimization problems and they are fast enough to be practical. These techniques form a weighted graph to

minimize the energy function, with two terminal vertices called the source and sink (Figure 4).

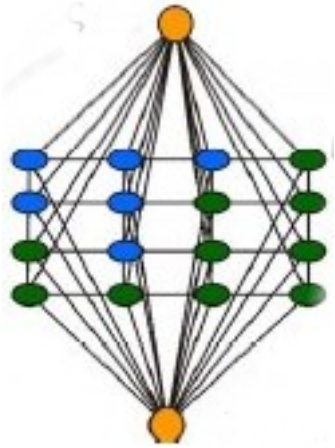

Figure 4: Graph with two terminal nodes (source and sink).

A *graph cut* is a set of edges that splits in two disjoint sets, each containing a terminal node. It can be seen that for a labelling problems with two-labels, each cut splits pixels and edges into two disjoint sets and thus corresponds to a valid solution of the labelling problem (Figure 5). In weighted graphs, where a weight is assigned to each edge, the *cost of the cut* is defined to be the sum of weights of the edges belonging to the cut.

The minimum cut problem is to find the cut with the minimum cost, which minimizes the energy either globally or locally. The minimum cut, in turn, can be computed very efficiently by max flow algorithms.

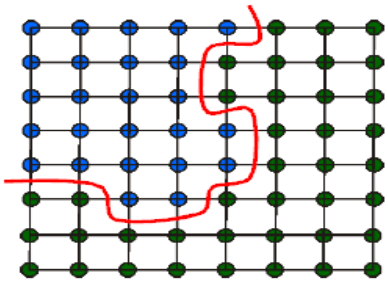

Figure 5: A graph cut solves the image segmentation problem by splitting pixels and edges into two disjoint sets

The α-expansion and the α-β-swap algorithms, introduced by Y. Boykov et al [50], are two of the most efficient algorithms for minimizing discontinuity-preserving energy functions. These algorithms can change simultaneously the labels of arbitrarily large sets of pixels. This makes these algorithms computationally efficient when compared to standard energy optimization algorithms, like simulated annealing in which changes occur much more slowly.

For instance in α-expansion algorithm, the algorithm in each iteration selects a label α, and then finds a lower-energy configuration within a single alpha-expansion move. If this expansion move has indeed lower energy than the current labelling, it becomes the current labelling for the next iteration. The algorithm terminates with a labelling that is a local minimum of the energy [51].

A small introduction to graph theory and graph cuts can be found in the next section, followed by the description of segmentation approach that was used for the segmentation of microscope images.

2.4.4.1 Introduction to Graph Theory

Graph Theory is the study of Graphs. A Graph is a representation of a sequence of objects that are linked together with links. In other words, it's a diagram composed by nodes and links, or points and lines connecting these points. What is important in graphs is the points that are linked with each point. In contrast with other geometrical structures, their study does not include the type of the lines that act as links (e.g. if they are curves or straight lines), or the positions of the nodes in space. However, for visualization purposes, straight lines are usually used and neighbouring nodes are usually represented as points that are close to each other in space. Each link may or may not have a direction. If it does not have a direction, it is assumed to be bidirectional. Furthermore, a link can be characterized by its length. The length of the link is not necessarily equal to the length of the line that represents it. For example, a graph may represent a road network, in which the nodes are the cities. Elevation changes (mountains, hills, valleys, etc.) change the length of each link, without this being visualized in the map of the area.

A graph consists of a finite (and possibly mutable) set of ordered pairs, called edges or arcs, of certain entities called nodes or vertices. As in mathematics, an edge (x,y) is said to point or go from x to y. The nodes may be part of the graph structure, or may be external entities represented by integer indices or references.

A graph G=(V,E) consists of a set of nodes (or vertices)V and a set of edges E .Each edge is defined as an unordered pair of two nodes:

$$E \subseteq V \times V$$

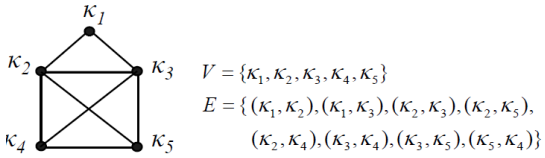

Figure 6: A Graph example

The edges may be directed (asymmetric) or undirected (symmetric). In the first case the graph is called *ordered* and in the second case they are called *unordered*. In mathematical notation, the definition of a graph is as follows: Graph G is an ordered pair G=<V(G), E(G)> where:

V(G)={v1,v2...vn} is the set of vertices

E(G)={e1,e2...em} is the set of edges

In the case of an unordered graph, each edge is a set that consists of two members (the two vertices), which are called terminal vertices (nodes) and they are not necessarily different from each other. In the case of an ordered graph, each edge is an ordered pair that of two vertices.

A *weighted graph* is a graph where a value (weight) has been assigned to each edge.

A graph G=(V,E) can alternatively be represented by an |V | × |V | *adjacency matrix* with each element $a_{i,j}$(where j<|V |) is defined as:

$$a_{i,j} = \begin{cases} 1, & if\ (i,j) \in E \\ 0, & othewise \end{cases}$$

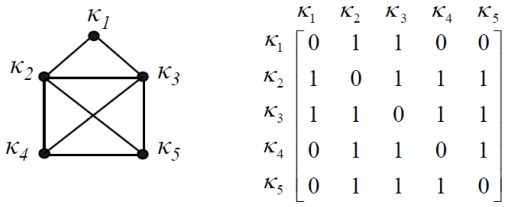

Figure 7: Example of the adjaceny matrix of a graph

2.4.4.2 Segmentation using Graph Cuts

In the method that was implemented for the segmentation of microscopy images, the energy minimization approach by Y. Boykov et al [49] was used to find the solution of the two-label (foreground/background) segmentation problem. The main steps of the algorithm are the following:

1. A k-means clustering algorithm was used to segment the colour image into two distinct sets.
2. The covariance matrices are computed for each class and are used to find the Mahalanobis distance of each sample from the center of the class.
3. The energy minimization problem is formulated to optimally re-assign labels to all pixels forcing also smoothness constraints. Specifically, a) the data term was chosen as minus the log likelihood of the pixel to belong to each class b) a fixed smoothing cost is applied to each two neighbouring pixels with dissimilar label and a spatially varying smoothness cost is assigned, that assigns a smaller cost to image edges (detected by filtering the image using a Sobel mask).
4. The minimum cut is found by performing α-expansion iterations until convergence or until a maximum number of iterations has been reached. The α-β-swap algorithm can also be used as an alternative to the this technique.

2.5 Splitting spatially clustered groups of cells using Distance transformation and the Watershed algorithm

After the application of image segmentation techniques, the image can be converted to a binary image, where black pixels correspond to foreground (cells) and white pixels correspond to background (collagen).

Morphological operations (e.g. dilation or erosion) followed by a connected component labelling procedure are performed to identify and label each individual cell.

However, a common problem that can occur after the image segmentation is that spatially clustered cells that are touching or even overlapping each other may be merged together as one cell. For such cases, we chose to use a relatively simple technique to split them into individual cells based on the resulting binary image for these cells (binary mask) and the watershed algorithm.

Specifically, we first apply a distance transformation within each of these large cell groups followed by a watershed algorithm, which can then split these groups of cells to identify each individual cell. Below, an introduction of the watershed algorithm for grey level images is described.

2.5.1 Watershed algorithm

The watershed algorithm is a morphological segmentation tool and belongs in the category of region-based image segmentation methods, which rely on the detection and merging of similar image pixels and regions, based on a specific feature. Beucher and Lantuejoul were the first to apply the Watershed transformation for image segmentation [47].

The watershed transformation represents the image as a surface where bright pixels (larger intensities) have higher values and dark pixels (lower intensities) have lower values. Image segmentation using the watershed transform performs better if we recognize the foreground objects and the background regions in the image.

An image can be viewed as a topographical relief surface. The higher the intensity of a pixel, the higher is its height in this surface S. If we assume that a drop of water falls on a point *p of surface* S then this will flow downwards following a path on the slide until the point where it will be trapped in a local minimum *M of the* topographical relief. The set *C(M) of the image pixels that have the property that when a drop of water falls on them will end to the same minimum M comprise a catchment basin of the local minimum M*. The set of boundaries of all the different basins of the image comprises its Watershed. In other words, the lines of the watershed lie on the ridgelines of the image, which actually enclose different local minima (Watershed lines are always closed).

The procedure with which the Watershed lines are identified is similar to a flooding of the relief. The relief, in which we have created holes in the points that correspond to the local minima, is gradually submerged in a basin of water. The water goes through the holes and floods the valleys. During this submerge, two or more floods that correspond to two or different local minima may be merged. To avoid this merge, a water barrier is built in at the points where the two floods would be merged. At the end of the procedure, i.e. when the entire image is submerged under the water, the only part that will be above the water level will be the water barriers, which define the watersheds and separate the basins, each containing only one local minimum.

2.6 Experimental Results

In 8(a), a 1201x901 H&E stained image is presented along with a manually marked ground truth mask 8(b).

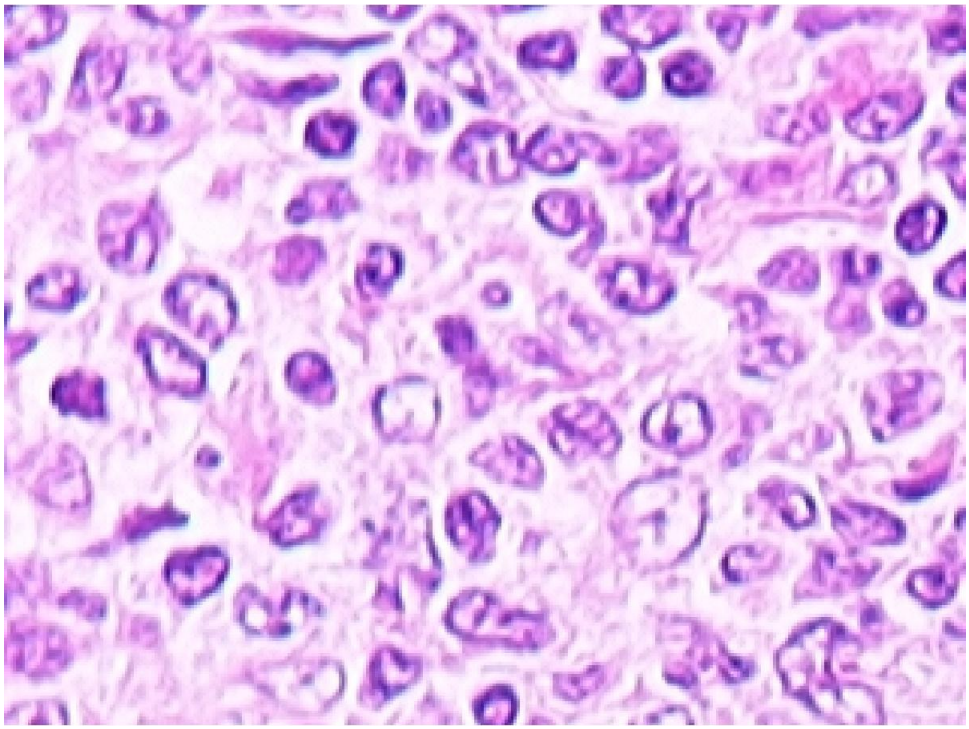

(a)

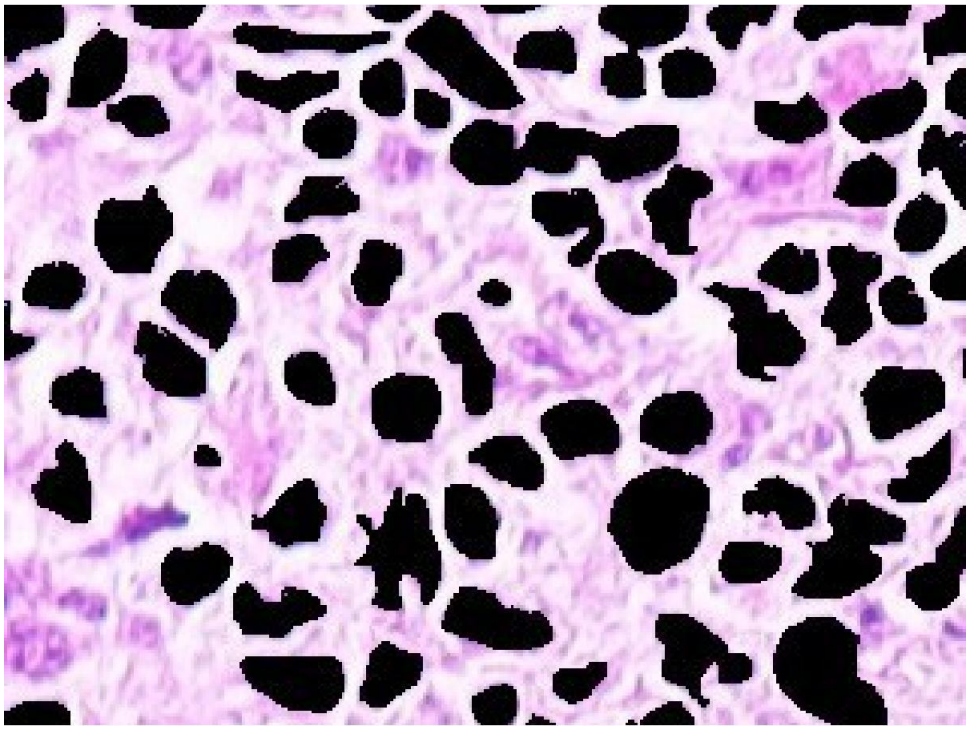

(b)

Figure 8: Original image and Ground truth mask

The average results for this image using each of the 7 segmentation methods are presented in Table 1. We regard as “positive” the foreground and as “negative” the background area. The number of true positives, false positives, true negatives, false negatives and the total number of pixels is reported.
Furthermore the precision, recall and F index are computed. Precision is defined as the number of true positives divided by the total number of positives ($\frac{tp}{tp+fp}$), while recall is defined as the number of true positives divided by the total number of successful classifications ($\frac{tp}{tp+fn}$). The F-index is defined as F=$\frac{2*precision*recall}{precision+recall}$) and is a good criterion to measure the efficiency of the classification.

Table 1: Evaluation of Image Segmentation Methods

Segmentation Methods	tp	fp	tn	fn	total	precision	recall	F
Otsu	259858	61972	669604	90667	1082101	0.807439	0.741339	0.772979
Kapur	160514	16021	715555	190011	1082101	0.909247	0.457925	0.609092
Iterative	263101	64197	667379	87424	1082101	0.803858	0.750591	0.776312
Isodata	263101	64197	667379	87424	1082101	0.803858	0.750591	0.776312
FCM Clustering	107046	7064	724512	243479	1082101	0.938095	0.305388	0.460775
Gaussian Mixture Model	120637	26347	705229	229888	1082101	0.820749	0.344161	0.484964
Graphcut	304266	108710	622866	46259	1082101	0.736764	0.868029	0.797028

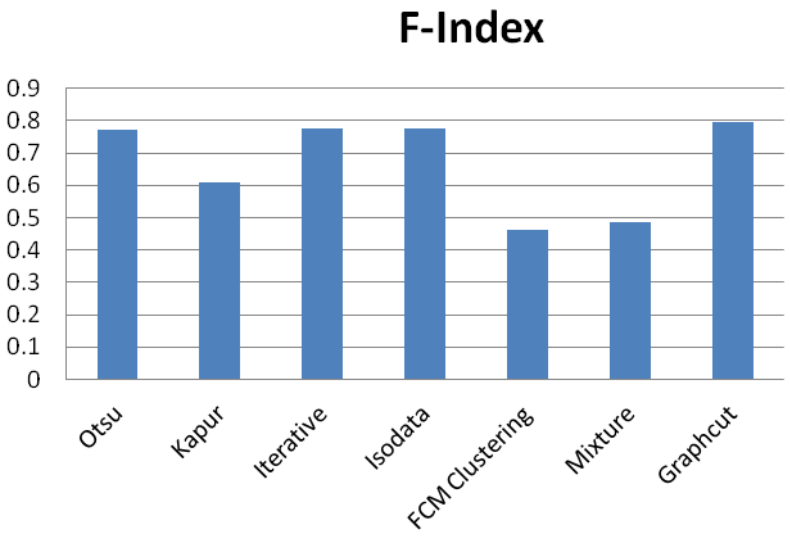

Figure 9: F-index for different segmentation methods

Detailed results for each segmentation method are shown below:

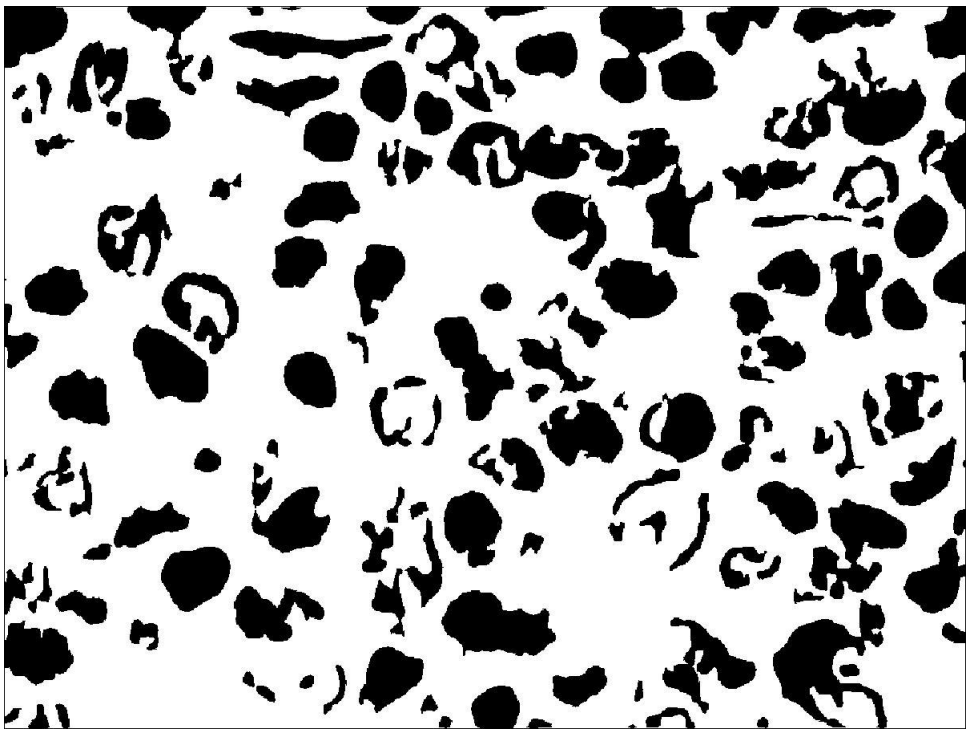

(a) Otsu

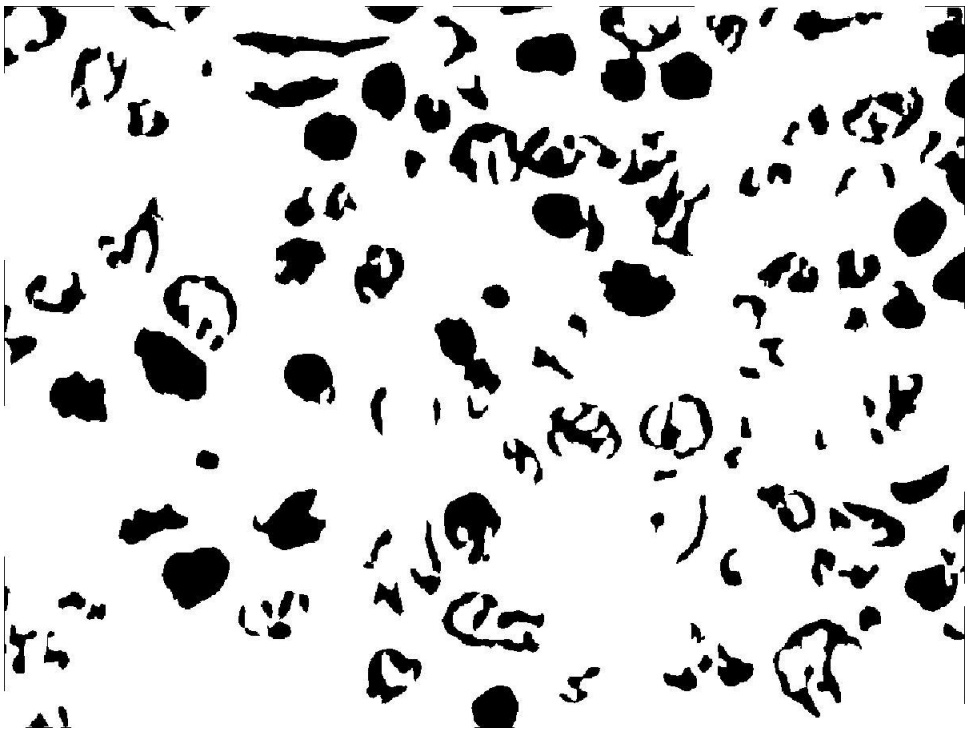

(b) Kapur

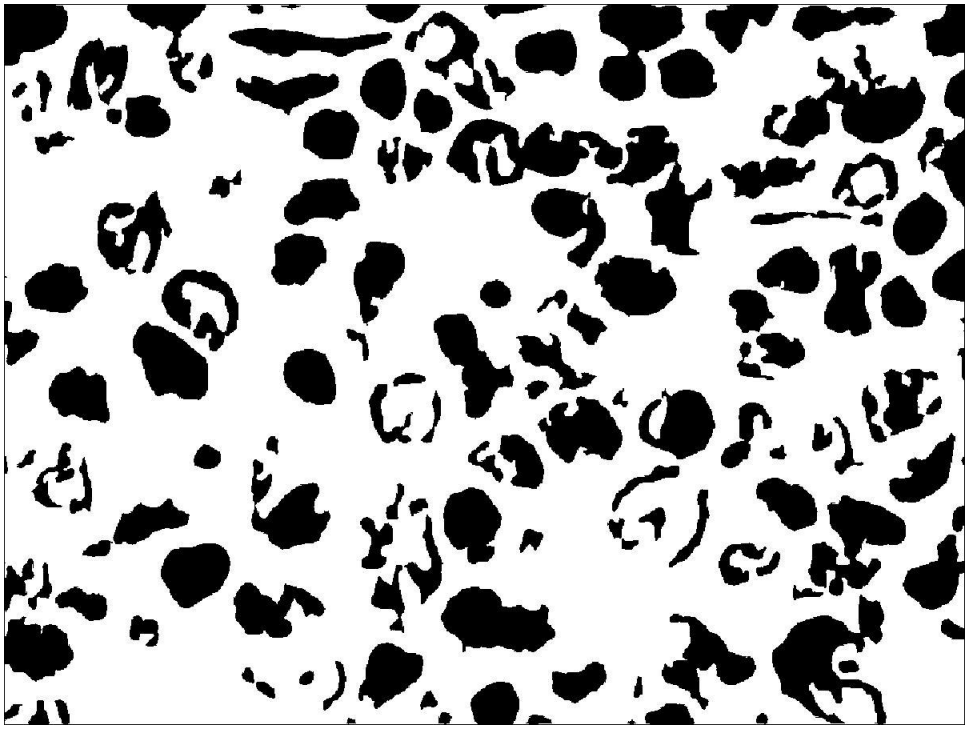

(c) Iterative

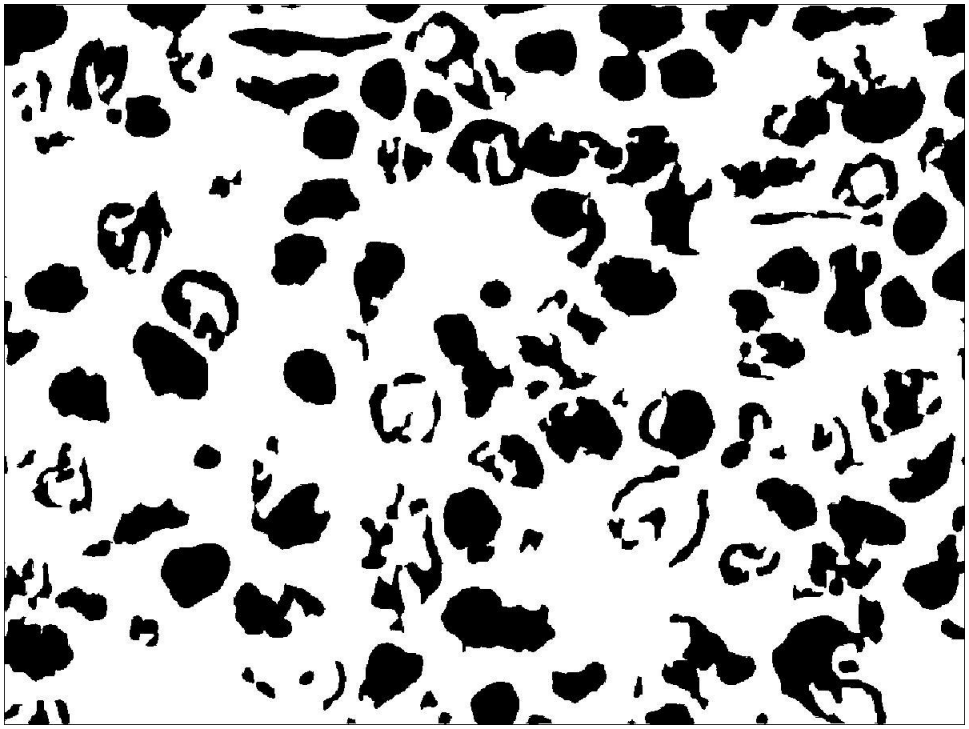

(d) ISODATA

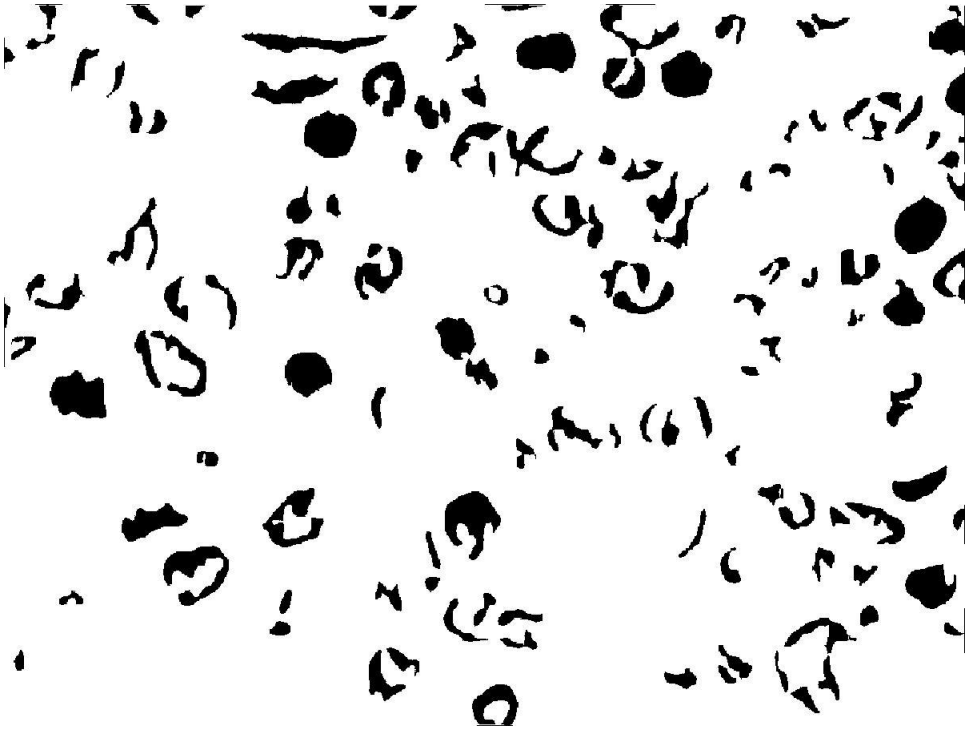

(e) FCM Clustering

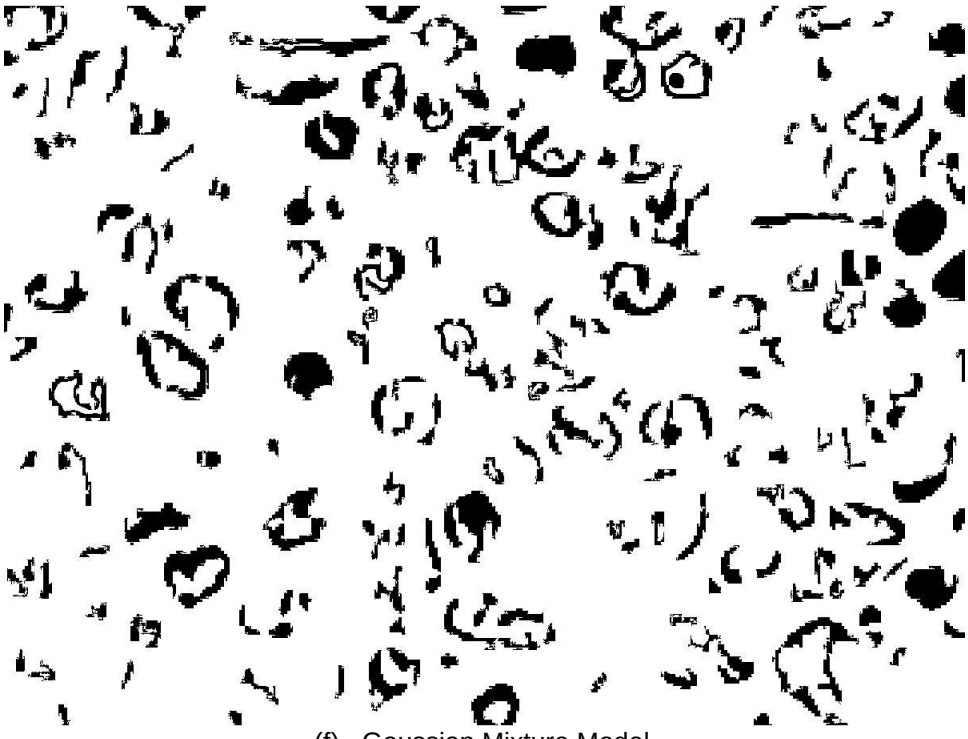

(f) Gaussian Mixture Model

(g) Graph Cuts

Figure 10: Segmentation results produce by the seven segmentation techniques (a-g)

From the results presented above (9), we can conclude that the segmentation based on graph cuts are the most efficient segmentation solution, while the Otsu, Iterative and ISODATA methods also provide very good segmentation results.

References:

[1] A. J. Mendez, P. G. Tahoces, M. J. Lado, M. Souto, and J. J. Vidal, "Computer-aided diagnosis: automatic detection of malignant masses in digitized mammograms," Med Phys, vol. 25, pp. 957-64, Jun 1998.

[2] J. Tang, R. Rangayyan, J. Xu, I. El Naqa, and Y. Yang, "Computer-Aided Detection and Diagnosis of Breast Cancer with Mammography: Recent Advances," IEEE Trans Inf Technol Biomed, Jan 20 2009.

[3] R. Rubin, D. Strayer, E. Rubin, and J. McDonald, Rubin's pathology: clinicopathologic foundations of medicine: Lippincott Williams & Wilkins, 2007.

[4] K. L. Weind, C. F. Maier, B. K. Rutt, and M. Moussa, "Invasive carcinomas and fibroadenomas of the breast: comparison of microvessel distributions--implications for imaging modalities," Radiology, vol. 208, pp. 477-83, Aug 1998.

[5] P. H. Bartels, D. Thompson, M. Bibbo, and J. E. Weber, "Bayesian belief networks in quantitative histopathology," Anal Quant Cytol Histol, vol. 14, pp. 459-73, Dec 1992.

[6] P. W. Hamilton, N. Anderson, P. H. Bartels, and D. Thompson, "Expert system support using Bayesian belief networks in the diagnosis of fine needle aspiration biopsy specimens of the breast," J Clin Pathol, vol. 47, pp. 329-36, Apr 1994.

[7] D. F. Gleason, "Histologic grading of prostate cancer: a perspective," Hum Pathol, vol. 23, pp. 273-9, Mar 1992.

[8] G. Alexe, G. S. Dalgin, D. Scanfeld, P. Tamayo, J. P. Mesirov, C. DeLisi, L. Harris, N. Barnard, M. Martel, A. J. Levine, S. Ganesan, and G. Bhanot, "High expression of lymphocyte-associated genes in node-negative HER2+ breast cancers correlates with lower recurrence rates," Cancer Res, vol. 67, pp. 10669-76, Nov 15 2007.

[9] M. Bibbo, D. H. Kim, T. Pfeifer, H. E. Dytch, H. Galera-Davidson, and P. H. Bartels, "Histometric features for the grading of prostatic carcinoma," Anal Quant Cytol Histol, vol. 13, pp. 61-8, Feb 1991.

[10] J. A. Belien, J. P. Baak, P. J. van Diest, and A. H. van Ginkel, "Counting mitoses by image processing in Feulgen stained breast cancer sections: the influence of resolution," Cytometry, vol. 28, pp. 135-40, Jun 1 1997.

[11] T. Markiewicz, S. Osowski, J. Patera, and W. Kozlowski, "Image processing for accurate cell recognition and count on histologic slides," Anal Quant Cytol Histol, vol. 28, pp. 281-91, Oct 2006.

[12] Y. J. Kim, B. F. Romeike, J. Uszkoreit, and W. Feiden, "Automated nuclear segmentation in the determination of the Ki-67 labeling index in meningiomas," Clin Neuropathol, vol. 25, pp. 67-73, Mar-Apr 2006.

[13] J. K. Sont, W. I. De Boer, W. A. van Schadewijk, K. Grunberg, J. H. van Krieken, P. S. Hiemstra, and P. J. Sterk, "Fully automated assessment of inflammatory cell counts and cytokine expression in bronchial tissue," Am J Respir Crit Care Med, vol. 167, pp. 1496-503, Jun 1 2003.

[14] S. Naik, Doyle,S., Madabhushi A, Tomaszeweski,J., Feldman,M., "Automated Gland Segmentation and Gleason Grading of Prostate Histology by Integrating Low-, High-level and Domain Specific Information," in Workshop on Microscopic Image Analysis with Applications in Biology Piscataway, NJ, 2007.

[15] P. S. Karvelis, D. I. Fotiadis, I. Georgiou, and M. Syrrou, "A watershed based segmentation method for multispectral chromosome images classification," Conf Proc IEEE Eng Med Biol Soc, vol. 1, pp. 3009-12, 2006.
[16] S. Petushi, F. U. Garcia, M. M. Haber, C. Katsinis, and A. Tozeren, "Large-scale computations on histology images reveal grade-differentiating parameters for breast cancer," BMC Med Imaging, vol. 6, p. 14, 2006.
[17] D. C. Fernandez, R. Bhargava, S. M. Hewitt, and I. W. Levin, "Infrared spectroscopic imaging for histopathologic recognition," Nat Biotechnol, vol. 23, pp. 469-74, Apr 2005.
[18] L. E. Boucheron, Z. Bi, N. R. Harvey, B. Manjunath, and D. L. Rimm, "Utility of multispectral imaging for nuclear classification of routine clinical histopathology imagery," BMC Cell Biol, vol. 8 Suppl 1, p. S8, 2007.
[19] S. S. Singh, B. Qaqish, J. L. Johnson, O. H. Ford, 3rd, J. F. Foley, S. J. Maygarden, and J. L. Mohler, "Sampling strategy for prostate tissue microarrays for Ki-67 and androgen receptor biomarkers," Anal Quant Cytol Histol, vol. 26, pp. 194-200, Aug 2004.
[20] D. L. Weaver, D. N. Krag, E. A. Manna, T. Ashikaga, S. P. Harlow, and K. D. Bauer, "Comparison of pathologist-detected and automated computer-assisted image analysis detected sentinel lymph node micrometastases in breast cancer," Mod Pathol, vol. 16, pp. 1159-63, Nov 2003.
[21] D. Glotsos, P. Spyridonos, P. Petalas, D. Cavouras, P. Ravazoula, P. A. Dadioti, I. Lekka, and G. Nikiforidis, "Computer-based malignancy grading of astrocytomas employing a support vector machine classifier, the WHO grading system and the regular hematoxylin-eosin diagnostic staining procedure," Anal Quant Cytol Histol, vol. 26, pp. 77-83, Apr 2004.
[22] C. Wahlby, I. M. Sintorn, F. Erlandsson, G. Borgefors, and E. Bengtsson, "Combining intensity, edge and shape information for 2D and 3D segmentation of cell nuclei in tissue sections," J Microsc, vol. 215, pp. 67-76, Jul 2004.
[23] V. R. Korde, G. T. Bonnema, W. Xu, C. Krishnamurthy, J. Ranger-Moore, K. Saboda, L. D. Slayton, S. J. Salasche, J. A. Warneke, D. S. Alberts, and J. K. Barton, "Using optical coherence tomography to evaluate skin sun damage and precancer," Lasers Surg Med, vol. 39, pp. 687-95, Oct 2007.
[24] M. Gurcan, T. Pan, H. Shimada, and J. H. Saltz, "Image analysis for neuroblastoma classification: Hysteresis thresholding for cell segmentation," in APIII 2006 Vancouver, BC, 2006.
[25] M. N. Gurcan, T. Pan, H. Shimada, and J. Saltz, "Image analysis for neuroblastoma classification: segmentation of cell nuclei," Conf Proc IEEE Eng Med Biol Soc, vol. 1, pp. 4844-7, 2006.
[26] P. Bamford and B. Lovell, "Method for accurate unsupervised cell nucleus segmentation," in Engineering in Medicine and Biology Society, 2001. Proceedings of the 23rd Annual International Conference of the IEEE, 2001, pp. 2704-2708 vol.3.
[27] G. Begelman, M. Pechuk, E. Rivlin, and E. Sabo, "System for Computer-Aided Multiresolution Microscopic Pathology Diagnostics," in Computer Vision Systems, 2006 ICVS '06. IEEE International Conference on, 2006, pp. 16-16.
[28] S. Naik, Doyle, S, Agner, S, Madabhushi, A, Tomaszeweski, J, Feldman, M, "Automated gland and nuclei segmentation for grading of prostate and breast cancer histopatholog," in ISBI Special Workshop on Computational Histopathology (CHIP) Paris, France: IEEE, 2008, pp. 284-287.
[29] J. A. Sethian, Level Set Methods: Evolving Interfaces in Geometry, Fluid Mechanics, Computer Vision and Materials Sciences, First ed.: Cambridge University Press, 1996.
[30] J. Kong, H. Shimada, K. Boyer, J. H. Saltz, and M. Gurcan, "Image analysis for automated assessment of grade of neuroblastic differentiation," IEEE International Symposium on Biomedical Imaging (ISBI) 2007, April 12-15, 2007, Metro Washington, D.C. , 2007.
[31] A. Can, M. Bello, X. Tao, M. Gerdes, A. Sood, M. Montalto, and F. Ginty, "Techniques for cellular quantitation of cancer biomarkers," in Microscopic Image Analysis for Life Science Applications: Artech House, 2008.
[32] Milan Zorman, Peter Kokol, Mitja Lenic, Jose Luis Sanchez de la Rosa, Jose Francisco Sigut, and Silvia Alayon. 2007. Symbol-Based Machine Learning Approach for Supervised Segmentation of Follicular Lymphoma Images. In *Proceedings of the Twentieth IEEE International Symposium on Computer-Based Medical Systems* (CBMS '07). IEEE Computer Society, Washington, DC, USA, 115-120. DOI=10.1109/CBMS.2007.105
[33] O. Sertel, G. Lozanski, A. Shanaah, and M.N. Gurcan, "Computer-aided detection of centroblasts for follicular lymphoma grading using adaptive likelihood based cell segmentation," *IEEE Trans. on Biomedical Engineering*, vol. 57(10), pp. 2613-2616, 2010.
[34] Kamel Belkacem-Boussaid, Jeffrey Prescott, Gerard Lozanski and Metin N. Gurcan, "Segmentation of follicular regions on H&E slides using a matching filter and active contour model", Proc. SPIE 7624, 762436 (2010); doi:10.1117/12.844285
[35] Kong H, Belkacem-Boussaid K, Gurcan MN, Partitioning Histopathological Images: An Integrated Framework for Supervised Color-Texture Segmentation and Cell Splitting**,** IEEE Transactions on Medical Imaging, (Accepted), 2011.
[36] Zhen Ma, João Manuel R. S. Tavares, and Renato M. Natal Jorge, A Review on the Current Segmentation Algorithms for Medical Images, In: IMAGAPP, INSTICC Press (2009) , pp. 135-140.
[37] D. L. Pham, C. Xu, J. L. Prince, A Survey of Current Methods in Medical Image Segmentation, In Annual Review of Biomedical Engineering, Vol. 2 (2000), pp. 315-338.
[38] http://en.wikipedia.org/wiki/Segmentation_(image_processing)
[39] M. Sezgin and B. Sankur, "Survey over image thresholding techniques and quantitative performance evaluation," J. Electron. Imaging, Vol. 13, No. 1, pp. 146–165, Jan. 2004.
[40] Nobuyuki Otsu (1979). "A threshold selection method from gray-level histograms". IEEE Trans. Sys., Man., Cyber. 9 (1): 62–66. doi:10.1109/TSMC.1979.4310076
[41] Kapur, J. N., Sahoo, P. K. and Wong, A. K. C. «A New Method for Gray-Level Picture Thresholding Using the Entropy of the Histogram.» Computer Vision, Graphics and Image Processing 29 (1985) 273-285.
[42] N. Kapur. Maximum entropy models in science and engineering. Wiley Eastern, New Delhi, 1989.

[43] Nikolaos Papmarkos, Digital Image Processing & Analysis (in Greek), ISBN:978-960-92731-3-8
[44] Geoffrey H. Ball, David J. Hall (1965), Isodata: a method of data analysis and pattern classification, Technical Report, Stanford Research Institute, Menelo Park, United States. Office of Naval Research. Information Sciences Branch
[45] Bezdek, James C. (1981), Pattern Recognition with Fuzzy Objective Function Algorithms. ISBN 0306406713
[46] O. Sertel, G. Lozanski, A. Shana'ah and M. Gurcan, Computer-Aided Detection of Centroblasts for Follicular Lymphoma Grading Using Adaptive Likelihood-Based Cell Segmentation, IEEE Transactions On Biomedical Engineering, Vol. 57, No. 10, October 2010, pp.2613-2616.
[47] Serge Beucher and Christian Lantuéjoul, Use of watersheds in contour detection. In International workshop on image processing, real-time edge and motion detection (1979). http://cmm.ensmp.fr/~beucher/publi/watershed.pdf
[48] Bezdec, J.C., Pattern Recognition with Fuzzy Objective Function Algorithms, Plenum Press, New York, 1981.
[49] Shapiro, Linda G. & Stockman, George C. (2002). "Computer Vision". Prentice Hall. ISBN 0-13-030796-3
[50] Y. Boykov, O. Veksler, R. Zabih, "Fast Approximate Energy Minimization via Graph Cuts", IEEE Transactions on Pattern Analysis and Machine Intelligence, vol. 23, no. 11, pp. 1222-1239, 2001.
[51] V. Kolmogorov and R. Zabih. "What Energy Functions can be Minimized via Graph Cuts?", In European Conference on Computer Vision, 2002

Note: This report is partly based on Gurcan, M.N.; Boucheron, L.E.; Can, A.; Madabhushi, A.; Rajpoot, N.M.; Yener, B.; , "Histopathological Image Analysis: A Review," Biomedical Engineering, IEEE Reviews in , vol.2, pp.147-171, 2009. The first and fifth authors are members of OSU and WARWICK, respectively.